Efficient Quantum Simulations of Devices Based on 2D Materials Including Vertical Heterojunctions

A. Sanchez-Soares*, T. Kelly*, S.-K. Su†, E. Chen†, J.C. Greer‡ and G. Fagas§
*EOLAS Designs, Grenagh, Co. Cork T23 AK70, Ireland. Email: alfonso.sanchez@eolasdesigns.com
†Corporate Research, TSMC, Hsinchu 30075, Taiwan.
‡Nottingham Ningbo China Beacons Institute, University of Nottingham Ningbo, Ningbo 315100, China.
§Tyndall National Institute, UCC, Lee Maltings, Cork, T12 R5CP, Ireland.

2024 International Conference on Simulation of Semiconductor Processes and Devices (SISPAD) | 979-8-3315-1635-2/24/$31.00 ©2024 IEEE | DOI: 10.1109/SISPAD62626.2024.10733084

***Abstract*—We present a modelling framework that enables efficient exploration of the electrical performance of devices based on 2D material vertical heterojunctions. Electronic structure data from density functional theory (DFT) simulations is used to extract parameters for k.p Hamiltonians. Material models are then employed in device simulations based on non-equilibrium Green's functions (NEGF) for a quantum-mechanical description of charge transport. Electron-phonon scattering is included in order to account for dissipative phenomena as well as phonon-assisted interlayer charge transport. We demonstrate our methodology with an application to a Dirac-source field-effect transistor (DS-FET) design based on a monolayer molybdenum disulfide channel (ML-MoS2) with a graphene contact.**

***Index Terms*—NEGF, cold source, phonon scattering**

I. Introduction

Devices based on materials with reduced dimensionality are attractive candidates for post-silicon technologies due to their potential for increased packing density in integrated circuits. The layered nature of 2D materials represents an advantage for both mitigating variability issues, and ensuring excellent electrostatic control in ultra-scaled devices [1]. Over the past decades a wide range of 2D materials have been investigated for applications in optoelectronic devices, with several candidates exhibiting favorable carrier mobilities down to atomic thicknesses. Furthermore, their potential for device design is significantly expanded through to their remarkable ability to integrate with each other. In recent years, a number of device designs based on vertical heterojunctions between 2D materials have opened new possibilities for contact design, tunnelling junctions, and even novel switching mechanisms [2], [3]. The large number of potential material combinations as well as significant challenges posed by associated process engineering call for guidance from simulation techniques to efficiently screen device designs.

Simulation studies performed on devices based of 2D materials suggest formalisms beyond standard technology computer-aided design (TCAD) tools are required to accurately predict their electrical performance [4]. In this work, we present a TCAD framework that enables a computationally efficient workflow for rapidly evaluating the predicted performance of devices based on 2D materials including vertical heterojunctions (VHJ). Our methodology focuses on capturing relevant quantum mechanical effects by employing advanced formalisms while retaining high computational efficiency. In the following, we present a case study on a cold source device design based on a heterojunction between graphene and ML-MoS_2. We demonstrate our implementation's ability to accurately describe quantum transport phenomena previously reported using computationally demanding atomistic simulations, at a fraction of the computational cost and without the need for specialised hardware. We additionally include the effects of electron-phonon scattering and discuss its impact on the switching characteristics of DS-FETs.

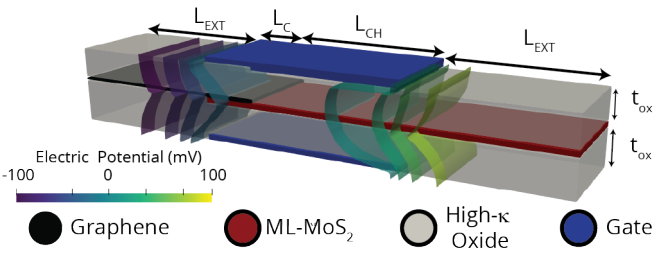

Fig. 1. Schematic of the double-gate device geometry studied. Top and bottom oxides are high-κ ($\varepsilon_r = 25$) with thickness t_{ox} = 3 nm. Source and drain extensions of length L_{EXT} = 15 nm are explicitly included in the self-consistent simulation loop. Top and bottom gates span the length of the ML-MoS_2 channel L_{CH} = 15 nm, and the length of the vertical contact L_C = 5 nm. Periodic boundary conditions are applied along the width direction. Overlaid contour surfaces correspond to electric potential for $V_{GS} \approx V_{Th}$.

II. Simulation Methodology

The electrical properties of the double-gate device design depicted in fig. 1 are simulated using the $\mathcal{Q}^*$ software package [5]. The DS-FET studied in this work is based on a graphene contact vertically coupled to ML-MoS_2, which comprises the channel and drain extension. Two layers of high-κ oxide ($\varepsilon_r = 25$) with $t_{ox} = 3$ nm thickness insulate active materials from top/bottom gate electrodes. The gated region extends the length of both the ML-MoS_2 channel ($L_{CH} = 15$ nm) and the VHJ ($L_C = 5$ nm). Degenerately doped regions are induced along lead extensions to form carrier reservoirs on either side of the channel. Lead extension regions with legths $L_{EXT} = 15$ nm are included in the explicit simulation domain. The ML-MoS_2 drain extension is doped n-type, while the

graphene source extension is doped p-type. Chemical doping is modeled using compensating charge densities homogeneously distributed along respective active material layers. Periodic boundary conditions are applied along the width direction to simulate infinitely wide devices.

The electrostatics and carrier transport equations are solved self-consistently in a Poisson-Schrödinger-NEGF loop within a coupled mode-space approach [6]. Relative permittivities of $\varepsilon_r^{\mathrm{Gph}} = 6.9$ and $\varepsilon_r^{\mathrm{MoS_2}} = 15.5$ are used within active materials when computing electrostatics [7], [8]. A recursive algorithm is used for efficient calculation of the Green's function when modeling charge transport [9]. The method includes explicit description of quantum effects in the active region such as source-drain tunneling and geometric scattering. The $\mathcal{Q}^*$ software package explicitly treats elastic and inelastic phonon scattering within the self-consistent Born approximation [10]. In this study we have used phonon deformation potentials for ML-MoS_2 and graphene reported in refs. [11], [12].

We model the electronic structure of each material in the vicinity of the K, K' valleys using $\vec{k} \cdot \vec{p}$ Hamiltonians defined as [13], [14]

$$\begin{aligned} \hat{H}_{\mathrm{Gph}} &= \hbar v_F \begin{pmatrix} 0 & k_- \\ k_+ & 0 \end{pmatrix} \\ \hat{H}_{\mathrm{MoS_2}} &= \begin{pmatrix} \varepsilon_{vb} + \alpha k^2 & \gamma k_- \\ \gamma k_+ & \varepsilon_{cb} + \beta k^2 \end{pmatrix}, \end{aligned} \tag{1}$$

where the energies of the valence and conduction bands in ML-MoS_2 are referred to the Dirac point in graphene, $\hbar$ is Planck's constant, the Fermi velocity v_F the γ parameter describe the isotropic dispersion around band edges, α/β break electron-hole symmetry, and $k_\pm = k_x \pm i k_y$. The interlayer interaction along the VHJ is modeled as

$$\hat{H}_{int} = \begin{pmatrix} t_v & t_i \\ t_i & t_c \end{pmatrix}. \tag{2}$$

A fitting module integrated into the $\mathcal{Q}^*$ software package is employed to extract all Hamiltonian parameters using electronic structure data from ab-initio simulations. Reference band structure data have been generated by DFT simulations using ultra-soft pseudopotentials as implemented in QUANTUM ESPRESSO [15], [16]. The non-local exchange-correlation functional vdW-DF3 is used in order to describe van der Waals interactions between graphene and ML-MoS_2 [17]. The band offsets of ML-MoS_2 and the elements of $\hat{H}_{int}$ are computed using a supercell including 5×5 unit cells of graphene and 4×4 unit cells of ML-MoS_2, where commensurability is enforced by applying 3.2% biaxial tensile strain to graphene.

III. RESULTS

Table I lists the continuum Hamiltonian parameters extracted from DFT data. Parameters for graphene and ML-MoS_2 have been extracted from simulations with isolated material layers. Figure 2 shows comparisons between band dispersions

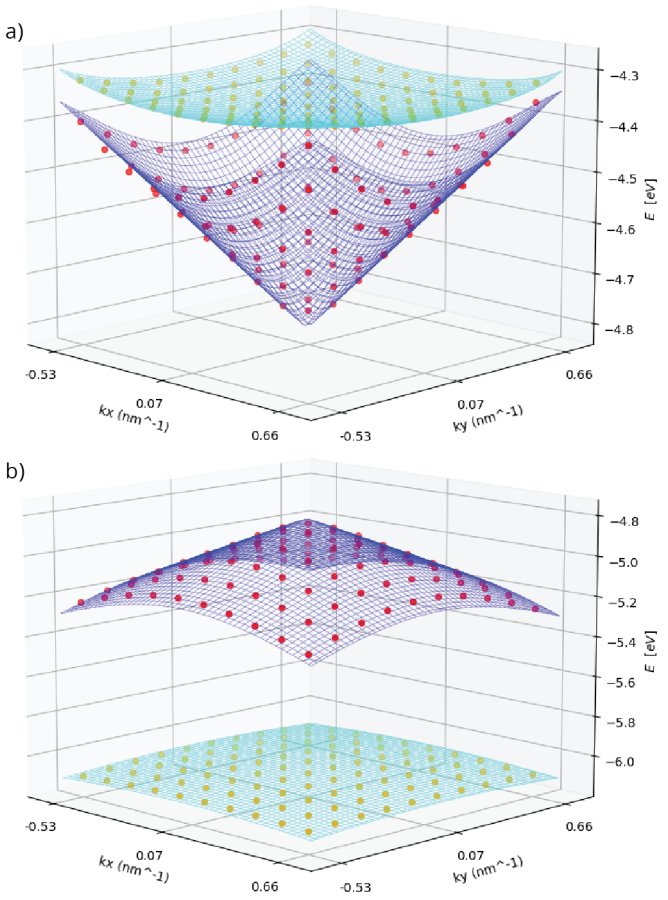

Fig. 2. Band structure for a Graphene/ML-MoS_2 vertical heterojunction near the Fermi level and around the K valley. Band edges for the a) conduction band and b) valence band computed with DFT (scatter plots), and with the continuum Hamiltonian employed for device simulations (mesh plots).

around the Fermi level of a graphene/ML-MoS_2 VHJ near the K valleys computed ab-initio, and with our fitted $\vec{k} \cdot \vec{p}$ model. Satisfactory agreement is achieved, with an l^2-norm of the fitting error of 3×10^{-4} eV, and maximum deviations around 15 meV found at points furthest from band extrema. The band alignment obtained from the VHJ simulation results in a barrier height of $\Phi_B = 0.428$ eV between graphene's Dirac point (DP) and the conduction band minimum (CBM) in ML-MoS_2. The tensile strain applied to graphene for the VHJ supercell results in a reduction of its Fermi velocity

TABLE I
HAMILTONIAN PARAMETERS FITTED FROM AB-INITIO SIMULATIONS.

	Parameter	Value
Graphene	v_F	8.3×10^5 m/s
Interlayer	t_v	0.030 eV
	t_c	0.013 eV
	t_i	-0.014 eV
ML-MoS_2	α	0.593 eV/Å^2
	β	1.264 eV/Å^2
	γ	3.66 eV/Å

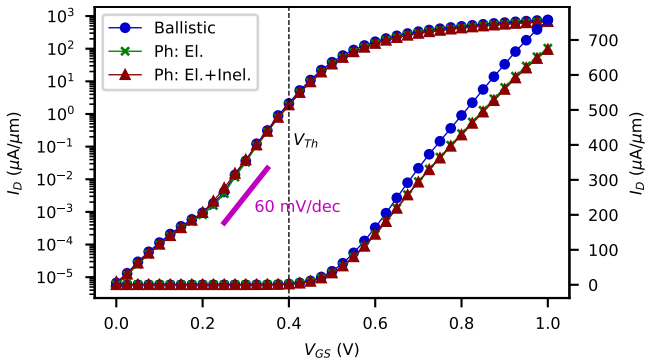

Fig. 3. Current-voltage characteristics simulated in the ballistic regime, with elastic phonon scattering, and with both elastic and inelastic phonon scattering. A threshold voltage of $V_{Th} = 0.4$ V has been extracted using the linear extrapolation method. Temperature is 300K.

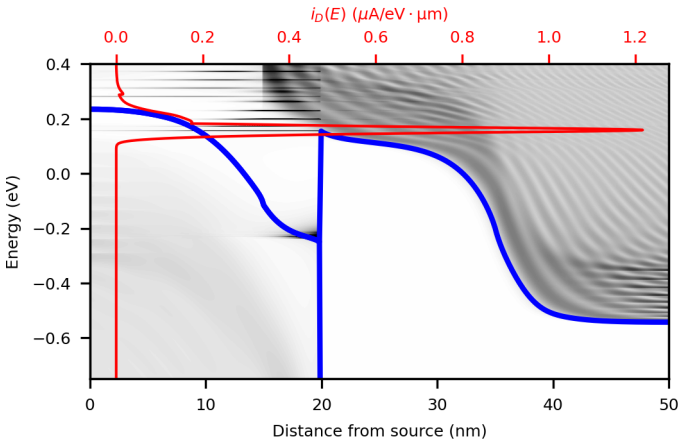

Fig. 5. Local density of states and spectral current in the ballistic approximation for $V_{GS} = 0.3$ V. Darker regions indicate larger density of states.

of approximately 7.9%. No other significant deviations from the electronic structure of isolated layers were observed. The magnitude of Hamiltonian elements describing interlayer coupling is found to be similar to those reported for bilayer MoS_2, in agreement with previous literature [18], [19].

Figure 3 shows the simulated transfer characteristics at a source-drain bias of $V_{DS} = 0.5$ V in the ballistic regime, when including inelastic phonon scattering, and when including the effects of both inelastic and elastic phonon scattering. The reduction in ON-state currents induced by phonon scattering increases with gate bias, up to around 8% at $V_{GS} = 1$ V. This reduction may be attributed to inelastic phonon scattering, given the negligible difference between transfer characteristics across both phonon models for $V_{GS} > V_{Th}$.

The impact of phonon scattering on states below threshold voltage is illustrated in fig. 4. In all cases, the subthreshold swing (SS) drops below the thermodynamic limit around $V_{GS} = 0.3$ V. Figure 5 shows the corresponding local density of states (LDoS) and spectral current in the ballistic approximation, where we can observe a minimum SS is achieved when the gate action swings the channel CBM below the graphene source's DP, in line with expected DS-FET behavior.

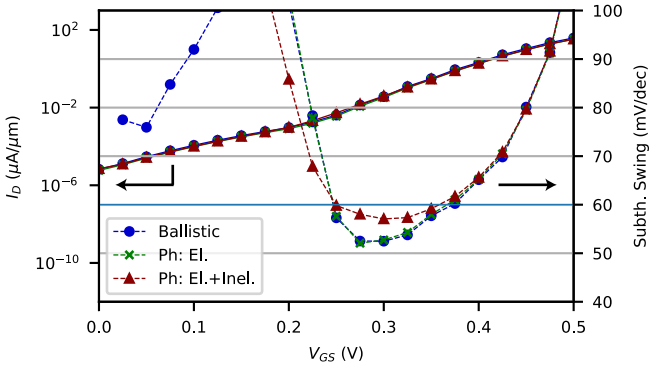

Fig. 4. Current and subthreshold swing versus gate bias in the ballistic limit, with elastic phonon scattering, and with both elastic and inelastic phonon scattering.

The energy dependence of the source density of states (DoS) modulates the rate at which electrons in graphene are able to overcome the barrier along the VHJ and into ML-MoS_2. As the gate bias increases and the channel CBM drops below the source DP, a decrease in source DoS with increasing energy results in sub-60 mV/dec switching [19]. The *sharpness* of the source DoS energy profile thus impacts the minimum SS that may be achieved. Since the source DoS is characterized by graphene's Fermi velocity, the SS dependence with gate bias is found to depend significantly on the value used in our simulations. Strategies that modify the DoS in graphene, such as strain engineering, may improve switching in DS-FET designs.

Although no significant variations in OFF currents are observed in fig. 4 when including phonon scattering, the introduction of inelastic scattering processes modifies the device switching characteristics. The impact of inelastic phonon scattering on current results in a smoother SS dependence with gate bias with respect to the ballistic / elastic scattering

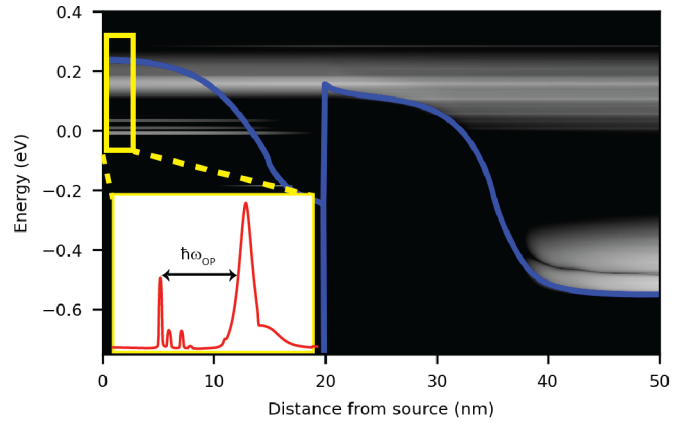

Fig. 6. Local spectral current when including elastic and inelastic phonon scattering for $V_{GS} = 0.3$ V. Brighter regions indicate larger spectral current. Inset illustrates peaks in the source side correspond to phonon absoption processes.

cases. The additional transport pathways enabled by inelastic scattering allow electrons in graphene with energies below the CBM to tunnel into channel, as illustrated in fig. 6. Absorption of optical phonons enable electrons in graphene with energies up to 0.2 eV below the CBM to contribute to current. The rate of carriers able to overcome the channel barrier is thus not solely determined by the source DoS at energies around the CBM. This results in an effective smearing of the source DoS, reducing the effectiveness of graphene's sharp DoS profile in achieving sub-60 mV/dec switching.

IV. Conclusion

We have presented an application of a framework that combines atomistic and continuum models to enable computationally efficient device simulations using state-of-the-art quantum formalisms. The capability of modeling devices based on 2D materials including vertical heterojunctions was illustrated by studying the electrical characteristics of a graphene/ML-MoS_2 DS-FET design. The electronic structure of graphene, ML-MoS_2, and associated heterojunction were modeled using $\vec{k} \cdot \vec{p}$ Hamiltonians parametrized from DFT simulations. Our description was found to reproduce ballistic transport characteristics previously reported using atomistic simulation methods. The effects of phonon scattering were assessed and found to degrade ON currents and significantly impact device switching characteristics. Inelastic phonon scattering was determined to be main mechanism behind ON current reduction. The bias dependence of the subthreshold swing was found to be smoothed by electron-phonon interactions, degrading the sub-60 mV/dec feature characteristic of DS-FETs. Current spectrum analysis reveals inelastic scattering in graphene to be the primary mechanism behind this effect. The methodology employed in this work aims to bridge the gap between TCAD and ab-initio simulations in order to minimize the use of ad-hoc parameters in an effort to provide enhanced physical insight. Facilitating rapid and accurate evaluation of device designs based on 2D materials and their combinations will be key in guiding experimental efforts on the road to achieving competitive post-silicon technologies.

References

[1] A. Liu, X. Zhang, Z. Liu, Y. Li, X. Peng, X. Li, Y. Qin, C. Hu, Y. Qiu, H. Jiang, Y. Wang, Y. Li, J. Tang, J. Liu, H. Guo, T. Deng, S. Peng, H. Tian, and T.-L. Ren, "The roadmap of 2D materials and devices toward chips," *Nano-Micro Letters*, vol. 16, no. 1, Feb. 2024.

[2] S. Kanungo, G. Ahmad, P. Sahatiya, A. Mukhopadhyay, and S. Chattopadhyay, "2D materials-based nanoscale tunneling field effect transistors: current developments and future prospects," *npj 2D Materials and Applications*, vol. 6, no. 1, Nov. 2022.

[3] C. Qiu, F. Liu, L. Xu, B. Deng, M. Xiao, J. Si, L. Lin, Z. Zhang, J. Wang, H. Guo, H. Peng, and L.-M. Peng, "Dirac-source field-effect transistors as energy-efficient, high-performance electronic switches," *Science*, vol. 361, no. 6400, pp. 387–392, Jun. 2018.

[4] A. Afzalian, "Ab initio perspective of ultra-scaled CMOS from 2D-material fundamentals to dynamically doped transistors," *npj 2D Materials and Applications*, vol. 5, no. 1, Jan. 2021.

[5] $\mathcal{Q}^*$ Simulator. (2024). EOLAS Designs. [Online]. Available: https://eolasdesigns.com/home/qstar/.

[6] M. Luisier, A. Schenk, and W. Fichtner, "Quantum transport in two- and three-dimensional nanoscale transistors: Coupled mode effects in the nonequilibrium Green's function formalism," *Journal of Applied Physics*, vol. 100, no. 4, p. 043713, Aug. 2006.

[7] J. Fang, W. G. Vandenberghe, and M. V. Fischetti, "Microscopic dielectric permittivities of graphene nanoribbons and graphene," *Physical Review B*, vol. 94, no. 4, p. 045318, Jul. 2016.

[8] T. Sohier, M. Calandra, and F. Mauri, "Two-dimensional Fröhlich interaction in transition-metal dichalcogenide monolayers: Theoretical modeling and first-principles calculations," *Physical Review B*, vol. 94, no. 8, p. 085415, Aug. 2016.

[9] M. Anantram, M. Lundstrom, and D. Nikonov, "Modeling of nanoscale devices," *Proceedings of the IEEE*, vol. 96, no. 9, pp. 1511–1550, Sep. 2008.

[10] A. Afzalian, "Computationally efficient self-consistent Born approximation treatments of phonon scattering for coupled-mode space non-equilibrium Green's function," *Journal of Applied Physics*, vol. 110, no. 9, Nov. 2011.

[11] X. Li, J. T. Mullen, Z. Jin, K. M. Borysenko, M. B. Nardelli, and K. W. Kim, "Intrinsic electrical transport properties of monolayer silicene and MoS_2 from first principles," *Physical Review B*, vol. 87, no. 11, p. 115418, Mar. 2013.

[12] T. Sohier, M. Calandra, C.-H. Park, N. Bonini, N. Marzari, and F. Mauri, "Phonon-limited resistivity of graphene by first-principles calculations: Electron-phonon interactions, strain-induced gauge field, and Boltzmann equation," *Physical Review B*, vol. 90, no. 12, p. 125414, Sep. 2014.

[13] P. Marconcini and M. M, "The $k \cdot p$ method and its application to graphene, carbon nanotubes and graphene nanoribbons: the Dirac equation," *Rivista del Nuovo Cimento*, 2011.

[14] A. Kormányos, G. Burkard, M. Gmitra, J. Fabian, V. Zólyomi, N. D. Drummond, and V. Fal'ko, "$\vec{k} \cdot \vec{p}$ theory for two-dimensional transition metal dichalcogenide semiconductors," *2D Materials*, vol. 2, no. 2, p. 022001, Apr. 2015.

[15] P. Giannozzi, O. Andreussi, T. Brumme, O. Bunau, M. Buongiorno Nardelli, M. Calandra, R. Car, C. Cavazzoni, D. Ceresoli, M. Cococcioni, N. Colonna, I. Carnimeo, A. Dal Corso, S. de Gironcoli, P. Delugas, R. A. DiStasio, A. Ferretti, A. Floris, G. Fratesi, G. Fugallo, R. Gebauer, U. Gerstmann, F. Giustino, T. Gorni, J. Jia, M. Kawamura, H.-Y. Ko, A. Kokalj, E. Küçükbenli, M. Lazzeri, M. Marsili, N. Marzari, F. Mauri, N. L. Nguyen, H.-V. Nguyen, A. Otero-de-la Roza, L. Paulatto, S. Poncé, D. Rocca, R. Sabatini, B. Santra, M. Schlipf, A. P. Seitsonen, A. Smogunov, I. Timrov, T. Thonhauser, P. Umari, N. Vast, X. Wu, and S. Baroni, "Advanced capabilities for materials modelling with QUANTUM ESPRESSO," *Journal of Physics: Condensed Matter*, vol. 29, no. 46, p. 465901, Oct. 2017.

[16] K. F. Garrity, J. W. Bennett, K. M. Rabe, and D. Vanderbilt, "Pseudopotentials for high-throughput DFT calculations," *Computational Materials Science*, vol. 81, pp. 446–452, Jan. 2014.

[17] D. Chakraborty, K. Berland, and T. Thonhauser, "Next-generation nonlocal van der Waals density functional," *Journal of Chemical Theory and Computation*, vol. 16, no. 9, pp. 5893–5911, Jul. 2020.

[18] A. Kormányos, V. Zólyomi, V. I. Fal'ko, and G. Burkard, "Tunable Berry curvature and valley and spin Hall effect in bilayer MoS_2," *Physical Review B*, vol. 98, no. 3, p. 035408, Jul. 2018.

[19] F. Liu, C. Qiu, Z. Zhang, L.-M. Peng, J. Wang, and H. Guo, "Dirac electrons at the source: Breaking the 60-mV/decade switching limit," *IEEE Transactions on Electron Devices*, vol. 65, no. 7, pp. 2736–2743, Jul. 2018.